

**Myocardial T₁ mapping at 5T using multi-inversion recovery
real-time spoiled GRE**

Linqi Ge¹, Huibin Zhu^{2,3}, Yihang Zhang¹, Lang Zhang¹, Yihang Zhou², Haifeng
Wang¹, Dong Liang^{1,2}, Hairong Zheng¹, Yanjie Zhu¹

¹Paul C. Lauterbur Research Center for Biomedical Imaging, Shenzhen Institute of Advanced
Technology, Chinese Academy of Sciences, Shenzhen, China

²Center for Medical AI, Shenzhen Institute of Advanced Technology, Chinese Academy of
Sciences, Shenzhen, China

³School of Mathematical Science, Inner Mongolia University, Hohhot, China

***Correspondence to:**

Yanjie Zhu, Ph.D.

Paul C. Lauterbur Research Centre for Biomedical Imaging

Shenzhen Institutes of Advanced Technology

Chinese Academy of Sciences, Shenzhen, Guangdong, China, 518055

Tel: (86) 755-86392243

Fax: (86) 755-86392299

Email: yj.zhu@siat.ac.cn

Running head: Myocardial T₁ mapping at 5 T

Word count: 4306

ABSTRACT

Purpose: To develop an accurate myocardial T_1 mapping technique at 5T using Look-Locker-based multiple inversion-recovery with the real-time spoiled gradient echo (GRE) acquisition.

Methods: The proposed T_1 mapping technique (mIR-rt) samples the recovery of inverted magnetization using the real-time GRE and the images captured during diastole are selected for T_1 fitting. Multiple-inversion recoveries are employed to increase the sample size for accurate fitting. Furthermore, the inversion pulse (IR) was tailored for cardiac imaging at 5T, optimized to maximize the inversion efficiency over specified ranges of B_1 and off-resonance. The T_1 mapping method was validated using Bloch simulation, phantom studies, and in 16 healthy volunteers at 5T.

Results: The optimized IR pulse based on the tangent/hyperbolic tangent pulse was found to outperform the conventional hyperbolic secant IR pulse within a limited peak amplitude of 10.6 μT at the 5T scanner. This optimized IR pulse achieves an average inversion factor of 0.9014 within a B_0 range of $\pm 250\text{Hz}$ and a B_1 range of -50% to 20%. In both simulation and phantom studies, the T_1 values measured by mIR-rt closely approximate the reference T_1 values, with errors less than 3%, while the conventional MOLLI sequence underestimates T_1 values. The myocardial T_1 values at 5T are 1553 ± 52 ms, 1531 ± 53 ms, and 1526 ± 60 ms (mean \pm standard deviation) at the apex, middle, and base, respectively.

Conclusion: The proposed method is feasible for myocardial T_1 mapping at 5T and provides better accuracy than the conventional MOLLI sequence.

Keywords: Myocardial T_1 mapping, 5T, Look-Locker

1. Introduction

Myocardial T_1 mapping can depict subtle variations in myocardium, allowing the detection of myocardial amyloidosis, iron overload, and myocardial infarction without using contrast agents^{1,2}. It has been widely used in clinical diagnosis and research at 1.5T and 3T. In recent years, although ultra-high field MR scanners, including 5T and 7T, have become popular around the world, cardiac imaging at ultra-high fields is still in its infancy.

Various techniques have been employed to quantify myocardial T_1 relaxation time, each having its own merits and limitations³. The most commonly used technique is the Modified Look-Locker Inversion Recovery (MOLLI) sequence and its derivations⁴⁻⁶. In MOLLI, single images are intermittently acquired during diastole gated by electrocardiogram in 3 to 5 heartbeats following the inversion pulse (IR), resulting in images spaced along T_1 recovery curves at RR interval. Then the images acquired after multiple IRs are concatenated together for T_1 curve fitting using the Look-Locker model. However, MOLLI-based sequences would underestimate T_1 values at 5T. The main reason is that 5T has a longer T_1 relative to 3T, and the duration of skipped heartbeats is insufficient for complete magnetization recovery. The previous study has illustrated that myocardial T_1 mapping at 7T requires an extended skipped heartbeat number for accurate measurement, at the cost of prolonging the scan time⁷. Saturation Recovery Single-Shot Acquisition (SASHA)⁸ provides an alternative to overcome this issue but suffers from limited signal-to-noise ratio (SNR) and precision. The longer T_1 at 5T makes this issue even worse. STONE sequence⁹ can achieve accurate T_1 measurement with high SNR but must acquire five slices together.

For myocardial T_1 mapping at 5T, the issue of B_1+ inhomogeneity should be seriously considered. At ultra-high fields, interference effects cause severe B_1+ inhomogeneity because the wavelength of RF becomes equal to or shorter than the dimensions of typical organs of interest¹⁰, especially in cardiac and abdomen imaging. Therefore, flip angle-related T_1 mapping techniques, such as the variable flip angle method^{11,12}, may not be suitable. Additionally, due to the high SAR value and susceptibility to B_0 inhomogeneity, the conventionally used balanced steady-state free precession (bSSFP) readout is typically replaced by the spoiler gradient echo (GRE) in ultra-high field cardiac imaging.

Considering all the above issues, we rethought the Look-Locker technique that samples the T_1 recovery by a continuous GRE acquisition following the IR. The increased T_1 at 5T allows a broader acquisition window for sampling the T_1 recovery. Furthermore, the Look-Locker technique has low SAR and is less sensitive to the B_1+ inhomogeneity due to the inherent low flip angle of GRE, making it suitable for ultra-high fields. Therefore, we propose a multi-inversion recovery Look-Locker method (mIR-rt) for myocardial T_1 mapping at 5T. The mIR-rt sequence employs real-time GRE to capture the recovery of inverted magnetization. Diastolic phase images are retrospectively selected based on the time stamps of raw data for T_1 fitting. Multi-inversions are used to increase the samples further. Besides, the IR was also optimized for cardiac imaging at 5T to achieve the maximum inversion efficiency. The accuracy of mIR-rt was thoroughly examined through simulations covering a wide range of T_1 values. Then the results were validated in a phantom study and 16 healthy volunteers.

2. Methods

2.1 Sequence

The mIR-rt sequence was implemented on a 5T scanner (Jupiter, United Imaging Healthcare, China). Figure 1 shows its timing diagram. In the sequence, real-time GRE acquisition is performed after an IR pulse to sample the recovery of longitudinal magnetization. After the spins reach the steady state (see Figure S1), a second IR pulse is applied, followed by real-time GRE acquisition to increase the number of data points. Finally, images acquired during diastole are selected for T_1 fitting. Specifically, 40 images are acquired between the first and second IR pulses, and 20 images are acquired after the second IR pulse. The first IR is gated by ECG with a trigger delay at diastole. This ensures that initial magnetization recovery is sampled during diastole, which is crucial for fitting accuracy. The total scan time is fixed and does not vary with heartbeats. Parallel imaging is used to reduce the scan time per image so that more data points can be acquired within the limited sampling interval for T_1 curve fitting. Since images in systolic are discarded for cardiac T_1 fitting, a second IR is applied followed by the real-time GRE to increase the data points.

TGRAPPA is used to reconstruct the k-space data. The calibration k-space lines needed to derive the coil sensitivity maps are obtained by averaging the k-space data of the last ten images.

The data acquired at the start of magnetization recovery is not used since the signal intensity varies dramatically. To improve the robustness of T_1 estimation, phase-sensitive inversion recovery reconstruction¹³ is employed to restore the polarity of MR signals after inversion with the phase of the last image as a reference.

2.2 T_1 fitting

The T_1 fitting model is derived from the Look-Locker method¹⁴. During real-time GRE acquisition, the recovery of longitudinal magnetization can be written as a mono-exponential relaxation curve,

$$M(t) = M_\infty - (M_\infty - M(0))\exp(-t/T_1^*), \quad [1]$$

where $M(0)$ is the initial longitudinal magnetization and M_∞ is the steady state signal of the GRE sequence. T_1^* denotes the apparent relaxation time. Let M_0 be the equilibrium magnetization. The inversion recovery of the first IR in mIR-rt sequence starts from $-\delta M_0$, where δ is the inversion efficiency (InvE). Substituting $M(0) = -\delta M_0$ into Eq.[1], the magnetization after the first IR can be characterized as:

$$M_1(t) = M_\infty - (M_\infty + \delta M_0)\exp(-t/T_1^*), \quad [2]$$

Similarly, the initial value following the second IR is $-\delta M_\infty$, assuming that the magnetization has reached the steady state of GRE before the second IR. The corresponding magnetization can be written as:

$$M_2(t) = M_\infty - (M_\infty + \delta M_\infty)\exp(-t/T_1^*), \quad [3]$$

From¹⁴, we know that m_∞ can be approximated by T_1^*/T_1 when $T_R \ll T_1^* < T_1$. Substituting m_∞ into Eq.[2] and [3] and combining them, the formula becomes

$$\begin{cases} M_1(t) = M_0^* - (\delta M_0 + M_0^*) \cdot \exp(-t/T_1^*) \\ M_2(t) = M_0^* - M_0^*(\delta + 1) \cdot \exp(-t/T_1^*) \end{cases} \quad [4]$$

where $M_0^* = M_0 T_1^*/T_1$. Let $A = M_0^* = M_0 T_1^*/T_1$ and $B = M_0(\delta + T_1^*/T_1)$. Eq.[4] can be written as

$$\begin{cases} M_1(t) = A - B \cdot \exp(-t/T_1^*) \\ M_2(t) = A - A(\delta + 1) \cdot \exp(-t/T_1^*) \end{cases} \quad [5]$$

In the above equation, there are four unknowns A , B , δ , and T_1^* that need to be determined. To improve fitting robustness, the inversion efficiency δ is estimated by the ratio of image intensities immediately before and after the second inversion pulse first. Then A , B , and T_1^* can be obtained by a three-parameter nonlinear fitting from Eq.[5]. Finally, T_1 can be

calculated by

$$T_1 = T_1^*(B/A - 1)/\delta, \quad [6]$$

In real scans, the dummy time Δt between the inversion and the start of the acquisition induces a systematic error, and the T_1 value should be corrected by ¹⁵:

$$T_{1\text{corrected}} = T_1 + 2\Delta t, \quad [7]$$

From the images acquired during all cardiac phases, diastolic images are selected retrospectively based on timestamps in raw data for T_1 calculation. Before curve fitting, the myocardial region of the selected images is aligned using a deep-learning-based image registration method ¹⁶. T_1 map is then fitted pixel-by-pixel with Eq.[5].

2.3 Optimization of Inversion Pulse

The inversion efficiency of adiabatic IR is essential for myocardial T_1 mapping ¹⁷, depending on the T_1 and T_2 values of the myocardium, pulse parameters, and field inhomogeneities. Due to the SAR limitation at 5T, the maximum achievable B_1 value is 10.6 μ T (about 450kHz), which is much lower than the B_1 strength of the optimal IR pulse of myocardial mapping at 3T¹⁷. Therefore, the IR pulse at 5T needs to be redesigned to optimize the inversion efficiency. The range for B_0 was set from -250 Hz to 250 Hz, while the range for B_1 was from -50% to 20% relative to the current B_1 value. Two adiabatic designs considered in this study were the hyperbolic secant (HSn) ¹⁸⁻²¹ and tangent/hyperbolic tangent (Tan/Tanh) ^{19,20,22}. For HSn design, the formula is as follows:

$$\begin{cases} \omega_1(t) = B_1 \text{sech}(\beta(2t/T_p - 1)^n) \\ \Delta\omega(t) = A \tanh(\beta(2t/T_p - 1)^n) \end{cases} \quad (0 < t \leq T_p), \quad [8]$$

where T_p is the duration of the pulses, A is the amplitude of the frequency sweep, and β and n are pulse shape parameters. The parameter ranges were: $n = 1, 2, 4, \text{ and } 8$, $A=100\text{-}1500\text{Hz}$ in 100Hz step, and $\beta = \text{asech}(x)$ with $x = 0.005\text{-}0.02$ in steps of 0.005. For Tan/Tanh design, the formula is as follows:

$$\begin{cases} \omega_1(t) = B_1 \tanh(2\xi t/T_p) \\ \Delta\omega(t) = A(\tan(\kappa(2t/T_p - 1))/\tan(\kappa)) \end{cases} \quad (0 < t \leq T_p), \quad [9]$$

where and ξ and κ are pulse shape parameters. The parameter ranges of Tan/Tanh were: $A = 4000\text{-}15000\text{Hz}$ in 500Hz step, $\tan(\kappa) = 8$ to 30 in steps of 2, and $\xi = 2$ to 20 in steps of 2. The ranges and steps of the RF parameters were determined based on previous studies ^{17,23}. B_1 field strength was set to the maximum achievable value of 450kHz for all designs. Considering the

limits on SAR and achievable B_1 , we empirically set the RF duration (T_p) range from 8 to 30 ms in 1 ms increments for both HS_n and Tan/Tanh.

2.4 Simulations

The InvE for a variety of IR designs was calculated using the Bloch simulation with $T_1 = 1500$ ms and $T_2 = 40$ ms. The simulation was conducted with the mri-rf package in the Michigan Image Reconstruction Toolbox (MIRT) ²⁴. The equilibrium magnetization M_0 was set to 1, and InvE was calculated as the ratio of the simulated longitudinal magnetization after the IR pulse to M_0 . The InvE across the B_0 and B_1 imperfection ranges were averaged and the pulse parameter combination with the highest average InvE was identified as the optimized set of parameters.

Bloch simulations were also performed to investigate the performance of the proposed mIR-rt method on T_1 estimation accuracy, as well as its sensitivity to variations in InvE, T_1 , and flip angle (FA). The following scenarios were simulated to assess the dependence of T_1 accuracy on these three parameters: (1) FA = 7°, $T_2 = 40$ ms, T_1 values ranging from 400-2000 ms (100 ms increments), and InvE ranging from 0.5 to 1.0 (0.1 increment); (2) $T_2 = 40$ ms, InvE = 0.85, T_1 values ranging from 400-2000 ms (incremented by 100 ms), and FA ranging from 3° to 11° (incremented by 2°); Simulated heart rate was 75 bpm. Other imaging parameters were the same as in-vivo experiments. The MOLLI sequence with scheme 5(3)3 was also simulated to compare its T_1 estimation accuracy with the mIR-rt method. The TIs of MOLLI were 150 ms and 300 ms. Spoiled GRE was employed in MOLLI since conventional used bSSFP readout is sensitive to B_0 field inhomogeneity and has a high SAR issue at ultra-high field. The normalized errors of T_1 estimation of each sequence were calculated using:

$$\text{Normalized } T_1 \text{ error(\%)} = \frac{(T_1^{est} - T_1^{ref})}{T_1^{ref}} \times 100, \quad [10]$$

where T_1^{est} is the T_1 value estimation by mIR-rt or MOLLI and T_1^{ref} is the gold standard.

2.5 Phantom study

All experiments were carried out at a 5T MR scanner (Jupiter, United Imaging Healthcare, China). Phantom experiments were performed to evaluate the accuracy of T_1 measurements using the mIR-rt sequence. The T1MES phantom ²⁵, made of NiCl₂-doped agarose gel with

different concentrations to mimic different cardiac compartments, was scanned using a local transmit and 24-channel receiver knee coil. We first standardized its T_1 value using the IR-SE sequence with 14 TIs logarithmically spaced from 25 to 3000 ms²⁶. Imaging parameters were: TR/TE = 20s/15.6ms, FOV = 200×200 mm, in-plane resolution = 1.56×1.56 mm, and slice thickness = 8 mm. To account for incomplete inversion, T_1 values of IR-SE were determined by a three-parameter fitting model ($S(TI_i) = A - B \cdot \exp(-TI_i/T_1)$)²⁷, and served as the reference standard. The total acquisition time was approximately 10.8 hours.

The T_1 value of the TIMES phantom was also measured by mIR-rt and MOLLI sequences. mIR-rt acquired a total of 60 images, comprising 40 images after the first IR pulse and 20 images after the second one. The phase encoding lines of each image are 42. Each image took 162.5ms and the total scan time was 10.2 s. The dummy time Δt was 5.8ms. The acquisition scheme of the MOLLI sequence was 5(3)3 using Grappa with R = 2 and separated calibration line number = 24. Other imaging parameters were: flip angle = 7°, bandwidth = 400 Hz/pixel, TR/TE=3.87/1.61 ms. The simulated heart rate was 75 bpm.

2.6 In-vivo study

The technique was also validated in 16 healthy volunteers (13 males and 3 females, aged 24 ± 2 years), with ethical approval obtained from the Institutional Review Board (IRB). Informed consent was obtained from each participant before the scan. The 5T MR scanner uses an 8-channel volume transmit loop array for cardiac imaging²⁸. For each subject, B_1+ shimming of the heart region was performed using an improved magnitude least squares method dubbed Eff-MLS²⁹. A 24-channel phased-array abdominal coil was used for signal reception. mIR-rt and MOLLI were used to obtain T_1 maps with ECG gating under breath hold. The trigger delay of mIR-rt was set to half of the RR interval to ensure the acquisition starts in the diastolic phase. Other imaging parameters were the same as in the phantom study. Diastole for each heartbeat is determined by an empirical threshold applied to the RR interval calculated from the timestamps in the raw data. An image is classified as diastolic if its k-space center line is acquired between 50% and 95% of the RR interval. Typically, 26-30 images are left for myocardial T_1 map fitting after discarding systolic data. 6 volunteers were scanned twice in two separate MR examinations to test the reproducibility of mIR-rt and MOLLI sequences.

3. Analysis

3.1 Phantom study

In the phantom study, the region of interest (ROI) of each tube was manually delineated. The spin-echo T_1 values were averaged within each ROI to obtain a reference T_1 value (T_1^{ref}) for each tube. Tubes with T_1 values below 500 ms were excluded from the analysis as this study focuses specifically on tissues with longer T_1 values. For each T_1 mapping sequence, the average T_1 (T_1^{cal}) and corresponding standard deviation (T_1^{std}) were computed over each tube. The accuracy of the measured T_1 value was defined as the absolute difference between T_1^{ref} and T_1^{cal} , and the precision for each tube was defined as T_1^{std} ³⁰.

3.2 In-vivo study

For the in-vivo study, calculating InvE for each subject is time-consuming and prone to instability. To address this issue, we employed the strategy used in Shao's paper ³¹ to measure the InvE. Specifically, 5 subjects were selected from the recruited volunteers to establish the average InvE for native myocardial tissue. For each subject, the InvE was calculated by the ratio of average signal intensities within manually drawn ROIs between the 41st and 40th images, which are captured just before and after the second IR. To enhance the robustness, the ROIs for these two images were placed on the ventricular septum and were as similar as possible. The InvE used in the fitting equation (Eq.[5]) was set to the average InvE derived from the 5 volunteers.

To calculate the global T_1 values, endocardial and epicardial contours of the left ventricle were manually traced on the T_1 maps by scripts developed in MATLAB (R2016a, MathWorks, MA, USA). The average T_1 value within the myocardium was calculated as global T_1 . The reproducibility of the T_1 mapping sequence was assessed using Intraclass Correlation Coefficients (ICC) ³² for the apex, middle, and base, respectively.

4. Results

4.1 Simulations

The best HS_n design is achieved with $\beta = 0.02$, $A = 0.5$ kHz, $\text{power} = 2$, and $T_p = 10$ ms and the average InvE = 0.8916 over B_0 of ± 250 Hz and B_1 of -50% to 20% for B_1 , while the

parameters for the best Tan/Tanh design are $A = 10$ kHz, $K_s = 4$, $k = 22$, and $T_p = 8$ ms with an average InvE = 0.9014. The InvE versus B_1 and off-resonance are graphed in Figure 2 for the best designs of both HS_n and Tan/Tanh. The Tan/Tanh design exhibits higher inversion over a larger B_0 and off-resonance area than the HS_n design. Additionally, the IR using the Tan/Tanh design exhibits a broad transitional band, which is advantageous for maintaining the uniformity of the blood pool. Therefore, we employed the Tan/Tanh design in this study.

Figure 3 shows the simulation results indicating the variation of T_1 value measured by mIR-rt on T_1 , FA, and InvE. Figure 3(a) illustrates the T_1 errors in the estimations obtained by mIR-rt under different InvEs and T_1 values. The T_1 error reduces with the increase of InvE and T_1 values. For the T_1 values larger than 1000ms, the error is less than 1% even with a low InvE of 0.5. Figure 3 (b) shows the T_1 errors varying with different FAs. Similar to Figure 3(a), when the T_1 values larger than 1000ms, the normalized T_1 errors of all FAs are less than 0.5%. The increase of FA improves the accuracy of measured T_1 but reduces the dynamic range and SNR of the T_1 -weighted images (see Figure S2), which has an adverse effect on the accuracy of estimated T_1 in real scenarios. Considering the tradeoff, we chose $FA = 7^\circ$ in this study. Figure 3(c) and 3(d) present the T_1 errors of MOLLI sequence under different InvEs, FAs, and T_1 values. The T_1 error of MOLLI reduces with the increase of InvE and decrease of FA. MOLLI underestimates T_1 measurement in case of long T_1 values due to the incomplete recovery.

4.2 Phantom studies

Figure 4 shows the T_1 maps and bar graph of the T_1 values obtained by IR-SE, mIR-rt, and MOLLI sequences in the phantom study. The T_1 values of mIR-rt are close to the reference values of IR-SE, while MOLLI's T_1 values were much lower than the reference. Table 1 summarizes the accuracy and precision of mIR-rt and MOLLI sequences. We can see that mIR-rt has higher accuracy than MOLLI, while the precision of these two sequences is comparable.

4.3 In-vivo studies

The average InvE of 5 healthy volunteers was 0.85 for native myocardium^{31,33}. Therefore, InvE was set to be 0.85 in this study.

Figure 5 shows the representative T_1 maps of two volunteers using mIR-rt and MOLLI. As we expected, the T_1 values obtained using MOLLI are much lower than those from mIR-rt.

Please note that different colorbar ranges are employed for MOLLI and mIR-rt to clearly illustrate the maps. The average native myocardial T_1 values of 16 health volunteers were 1553 ± 52 ms, 1531 ± 53 ms, and 1526 ± 60 ms at the apex, middle, and base. The T_1 values measured by MOLLI (1350 ± 48 ms, 1349 ± 47 ms, and 1354 ± 45 ms at the apex, middle, and base) were significantly lower than those of mIR-rt with $p < 0.05$ for all three layers. The average T_1 value of the blood pool using MOLLI (1718 ± 165 ms) was also significantly lower than the T_1 value derived from mIR-rt (1979 ± 97 ms) with $p < 0.05$. Table 2 shows the T_1 values of 6 volunteers using mIR-rt sequence from two separate scans, which were used for reproducibility analysis. The yielded ICC values were 0.7516 for the apex (good reproducibility), 0.9777 for the middle (excellent reproducibility), and 0.8201 for the base (good reproducibility). These results demonstrate that the mIR-rt sequence method used in our study provides high reproducibility, particularly in the middle slices, supporting its practical relevance for myocardial T_1 mapping.

In the in-vivo experiments, we found inhomogeneity in myocardial T_1 maps, especially in the lateral wall. The main reason for this inhomogeneity is the reduced local B_1 values, which lead to significantly lower inversion efficiency than intended. Figure 6 shows the representative T_1 maps alongside their corresponding B_0 and B_1 maps. Notably, the lower B_1 value in the lateral wall results in a reduced T_1 value in this region (indicated by red arrows), even though the redesigned inversion pulse has mitigated some of the adverse effects of B_1 inhomogeneity.

5. Discussion

This study demonstrated the feasibility of mIR-rt for accurate native myocardial T_1 mapping at 5T. The T_1 value obtained from the new method is in good agreement with the value obtained using the standard IR-SE sequence in the phantom study. The use of multiple IRs improves the robustness of T_1 fitting and an in-vivo T_1 map can be obtained by mIR-rt around 10 seconds.

The imperfection of IRs can introduce systematic errors in T_1 evaluation. IR pulses are typically optimized for specific magnetic field strengths to achieve maximum inversion efficiency^{6,7}, as high inversion efficiency is crucial for minimizing these errors. As described in previous literature, inversion efficiency should be considered in T_1 fitting to ensure accurate estimation⁶. In myocardial T_1 mapping at 7T⁷, inversion efficiency is measured by acquiring additional images separately at least $5 \times T_1$ after inversion, which greatly prolongs the acquisition time. Another approach,

Instantaneous Signal Loss Simulation (InSiL), involves InvE in the T_1 fitting model but still needs to acquire an additional proton density-weighted image. In the mIR-rt method, the second IR pulse allows for the calculation of the InvE without the need for additional acquisitions. Since the spins reach a steady state before the second IR pulse, InvE can be calculated using the images obtained just before and after this pulse. As a result, our method eliminates the requirement for extra images.

Optimizing the adiabatic IR pulse at 5T improves not only the inversion efficiency but also the homogeneity of the blood pool in T_1 maps. During myocardial T_1 mapping, data acquisition following the IR pulse often spans multiple cardiac cycles, during which distal blood flows into the heart. However, field homogeneity outside the heart is generally less optimal than within it, as local shimming is performed specifically in the cardiac region at 5T. This discrepancy can adversely affect the uniformity of distal blood flow and the blood pool in the T_1 map. Using a broadband IR pulse helps maintain the uniformity of distal blood flow during the IR pulse. Figure 7 shows the T_1 maps obtained with mIR-rt using optimized HS_n and Tan/Tanh IR pulses, demonstrating that the blood pool with HS_n displayed less uniformity compared to that with the broadband Tan/Tanh pulse.

SAR is essential for cardiac imaging. SAR monitoring at the 5T scanner is based on a human SAR model database. Specifically, this database is based on fifteen human models, which were simulated using Sim4Life software with anatomical images and actual dimensions of the volume transmitting coil³⁴. For each subject in a real scan, an appropriate human SAR mode is selected from the database first according to the subject's information, including weight, age, height, and imaging part of the subject. Then the local SAR can be predicted using this human SAR model and the scanning protocol. This SAR monitoring ensures that the local SAR of the sequence does not exceed IEC standards.

The underestimation of MOLLI T_1 is attributable to three primary factors: (1) It uses the Look-Locker fitting model, which was initially developed for continuous gradient echo readouts; (2) It assumes complete recovery of longitudinal magnetization before the subsequent inversion pulse, which is not true for long T_1 tissues or patients with high heart rates; (3) It presumes an ideal inversion pulse, an assumption that is not accurate, especially at 5T. The proposed sequence improves these limitations by (1) Utilizing continuous GRE readouts, which

align more closely with the Look-Locker model compared to MOLLI; (2) Assuming that spins reach a steady state of GRE readout before the second IR, a condition that is more feasible than full recovery, especially for long T_1 tissues; and (3) Incorporating the effect of inversion efficiency in mIR-rt, which further improves the accuracy of T_1 fitting.

Inversion recovery with real-time sampling has been applied to T_1 mapping for a long time¹⁴. Radial acquisition with model-based reconstruction proposed recently^{35,36} is an alternative to Cartesian sampling in this study. Although the radial trajectory is more robust to motion, its image has a mixed contrast if the contrast varies during acquisition since all lines cross the k-space center. On the other hand, image registration for myocardial region alignment is essential for the quality of T_1 maps. The model-based reconstruction directly estimates the T_1 map from k-space data, requiring a complex motion-resolved procedure when applied to the myocardium³⁷. Therefore, we chose to reconstruct images and fit T_1 maps independently.

This study has several limitations. First, the precision of myocardial T_1 maps at 5T is reduced compared to 3T, as GRE readouts are used instead of bSSFP. Previous studies have also demonstrated this difference in T_1 mapping precision between GRE and bSSFP readout³⁸. Applying a denoising filter during image processing can improve T_1 value precision, a technique often used in commercial sequences. We plan to incorporate it into our post-processing pipeline for future improvements. Second, the temporal resolution of mIR-rt is somewhat limited due to the restricted acceleration rate of TGRAPP, which constrains the number of images available for T_1 fitting. To increase the number of fitting images, we utilized a wider diastolic selection window (approximately half of each cardiac cycle), typically selecting 26-30 images for fitting. Spatial variations of the heart region among these images were corrected using the image registration method. Since the acquisition time for the mIR-rt sequence is constant, patients with higher heart rates cover more heartbeats and still have enough images for T_1 fitting, despite fewer samples per heartbeat. We have verified that heart rate has little impact on the T_1 values estimated by mIR-rt sequence (see Figure S3). In future work, we aim to employ advanced fast imaging techniques, such as deep learning-based methods, to further improve the temporal resolution and image SNR of the sequence.

6. Conclusion

The proposed mIR-rt sequence demonstrates superior accuracy compared to MOLLI, and this study reports myocardial T_1 values at 5T for the first time. The optimized IR pulse achieves high inversion efficiency across a broad range of B_0 and B_1 fields, resulting in enhanced quality of the myocardial T_1 map. Furthermore, improving local B_1 homogeneity in the heart region at ultra-high fields is crucial, as B_1 field inhomogeneity significantly impacts inversion efficiency and, consequently, the uniformity of myocardial T_1 values.

Funding

This work was supported by the National Natural Science Foundation of China under grant nos. 62322119, 12226008, Shenzhen Science and Technology Program under grant no. RCYX20210609104444089, JCYJ20220818101205012. Also supported by the Key Laboratory for Magnetic Resonance and Multimodality Imaging of Guangdong Province under grant no.2023B1212060052.

Reference

1. Higgins DM, Keeble C, Juli C, Dawson DK, Waterton JC. Reference range determination for imaging biomarkers: Myocardial T_1 . *J Magn Reson Imaging*. 2019;50(3):771-778.
2. Petersen A, Nagel SN, Hamm B, Elgeti T, Schaafs LA. The influence of left bundle branch block on myocardial T_1 mapping. *Sci Rep*. 2024;14(1):5379.
3. Petrusca L, Croisille P, Augeul L, et al. Cardioprotective effects of shock wave therapy: A cardiac magnetic resonance imaging study on acute ischemia-reperfusion injury. *Front Cardiovasc Med*. 2023;10:1134389.
4. Messroghli DR, Radjenovic A, Kozerke S, et al. Modified Look-Locker inversion recovery (MOLLI) for high-resolution T_1 mapping of the heart. *Magn Reson Med*. 2004;52(1):141-6.
5. Sussman MS, Wintersperger BJ. Modified look-locker inversion recovery (MOLLI) T_1 mapping with inversion group (IG) fitting - A method for improved precision. *Magn Reson Imaging*. Oct 2019;62:38-45.
6. Kellman P, Hansen MS. T_1 -mapping in the heart: accuracy and precision. *J Cardiovasc Magn Reson*. 2014;16(1):2.
7. Rodgers CT, Piechnik SK, Delabarre LJ, et al. Inversion recovery at 7 T in the human myocardium: measurement of T_1 , inversion efficiency and B_1 (+). *Magn Reson Med*. 2013;70(4):1038-46.
8. Chow K, Flewitt JA, Green JD, et al. Saturation recovery single-shot acquisition (SASHA) for myocardial T_1 mapping. *Magn Reson Med*. 2014;71(6):2082-95.

9. Weingartner S, Roujol S, Akcakaya M, Basha TA, Nezafat R. Free-breathing multislice native myocardial T(1) mapping using the slice-interleaved T(1) (STONE) sequence. *Magn Reson Med.* 2015;74(1):115-124.
10. Lan L, Hu H, Sun W, et al. Feasibility of cardiovascular magnetic resonance imaging at 5T in comparison to 3T. *Research Square.* 2022. doi: <https://doi.org/10.21203/rs.3.rs-2171514/v1>.
11. Clique H, Cheng HL, Marie PY, Felblinger J, Beaumont M. 3D myocardial T1 mapping at 3T using variable flip angle method: pilot study. *Magn Reson Med.* 2014;71(2):823-9.
12. Guo R, Si D, Chen Z, et al. SATuration-recovery and Variable-flip-Angle-based three-dimensional free-breathing cardiovascular magnetic resonance T(1) mapping at 3 T. *NMR Biomed.* 2022;35(9):e4755.
13. Xue H, Greiser A, Zuehlsdorff S, et al. Phase-sensitive inversion recovery for myocardial T1 mapping with motion correction and parametric fitting. *Magn Reson Med.* 2013;69(5):1408-20.
14. Deichmann R, Haase A. Quantification of T1 Values by Snapshot-Flash Nmr Imaging. *J Magn Reson.* 1992;96(3):608-612.
15. Deichmann R. Fast high-resolution T1 mapping of the human brain. *Magn Reson Med.* 2005;54(1):20-27.
16. Huang C, Sun L, Liang D, et al. RS-MOCO: A deep learning-based topology-preserving image registration method for cardiac T1 mapping. *arXiv preprint arXiv:2410.11651.* 2024. doi: <https://doi.org/10.48550/arXiv.2410.11651>.
17. Kellman P, Herzka DA, Hansen MS. Adiabatic inversion pulses for myocardial T1 mapping. *Magn Reson Med.* 2014;71(4):1428-34.
18. Tannus A, Garwood M. Improved performance of frequency-swept pulses using offset-independent adiabaticity. *J Magn Reson.* 1996;120(1):133-137.
19. Tannús A, Garwood M. Adiabatic pulses. *NMR Biomed.* 1997;10(8):423-434.
20. Garwood M, DelaBarre L. The return of the frequency sweep: designing adiabatic pulses for contemporary NMR. *J Magn Reson.* 2001;153(2):155-177.
21. Tesiram YA. Implementation equations for HS_n RF pulses. *J Magn Reson.* 2010;204(2):333-339.
22. Hwang TL, van Zijl PCM, Garwood M. Fast broadband inversion by adiabatic pulses. *J Magn Reson.* 1998;133(1):200-203.
23. Yang Y, Wang C, Liu Y, et al. A robust adiabatic constant amplitude spin-lock preparation module for myocardial T1ρ quantification at 3 T. *NMR Biomed.* 2023;36(2):e4830.
24. Fessler JA. Michigan Image Reconstruction Toolbox (MIRT). <https://web.eecs.umich.edu/~fessler/code/>
25. Captur G, Gatehouse P, Keenan KE, et al. A medical device-grade T1 and ECV phantom for global T1 mapping quality assurance-the T(1) Mapping and ECV Standardization in cardiovascular magnetic resonance (TIMES) program. *J Cardiovasc Magn Reson.* 2016;18(1):58.

26. Stanisz GJ, Odrobina EE, Pun J, et al. T1, T2 relaxation and magnetization transfer in tissue at 3T. *Magn Reson Med.* 2005;54(3):507-512.
27. Gai ND, Stehning C, Nacif M, Bluemke DA. Modified Look-Locker T1 evaluation using Bloch simulations: human and phantom validation. *Magn Reson Med.* 2013;69(2):329-336.
28. Fang F, Luo W, Gong J, et al. An 8-channel transmit loop array for body imaging 9 at 5T. In *Proceedings of the 29th Scientific Meeting of ISMRM, Virtual, 2021.* Abstract 1573.
29. Jiaxu Li, Nan Li, Liqiang Zhou, et al. Efficient RF Shimming Strategies for Cardiac MRI at 5T. In *Proceedings of the 32nd Annual Meeting of ISMRM, Singapore, 2024.* p. 4013.
30. Roujol S, Weingärtner S, Foppa M, et al. Accuracy, precision, and reproducibility of four T1 mapping sequences: a head-to-head comparison of MOLLI, ShMOLLI, SASHA, and SAPPHIRE. *Radiology.* 2014;272(3):683-689.
31. Shao J, Nguyen KL, Natsuaki Y, Spottiswoode B, Hu P. Instantaneous signal loss simulation (InSiL): an improved algorithm for myocardial T1 mapping using the MOLLI sequence. *J Magn Reson Imaging.* 2015;41(3):721-729.
32. Böttcher B, Lorbeer R, Stöcklein S, et al. Global and Regional Test–Retest Reproducibility of Native T1 and T2 Mapping in Cardiac Magnetic Resonance Imaging. *J Magn Reson Imaging.* 2021;54(6):1763-1772.
33. Rodgers CT, Piechnik SK, DelaBarre LJ, et al. Inversion recovery at 7 T in the human myocardium: measurement of T1, inversion efficiency and B1+. *Magn Reson Med.* 2013;70(4):1038-1046.
34. Graesslin I, Homann H, Biederer S, et al. A specific absorption rate prediction concept for parallel transmission MR. *Magn Reson Med.* 2012;68(5):1664-1674.
35. Wang X, Roeloffs V, Klosowski J, et al. Model-based T(1) mapping with sparsity constraints using single-shot inversion-recovery radial FLASH. *Magn Reson Med.* 2018;79(2):730-740.
36. Wang X, Rosenzweig S, Scholand N, Holme HCM, Uecker M. Model-based reconstruction for simultaneous multi-slice T1 mapping using single-shot inversion-recovery radial FLASH. *Magn Reson Med.* 2021;85(3):1258-1271.
37. Wang X, Rosenzweig S, Roeloffs V, et al. Free-breathing myocardial T(1) mapping using inversion-recovery radial FLASH and motion-resolved model-based reconstruction. *Magn Reson Med.* 2023;89(4):1368-1384.
38. Jang J, Bellm S, Roujol S, et al. Comparison of spoiled gradient echo and steady-state free-precession imaging for native myocardial T1 mapping using the slice-interleaved T1 mapping (STONE) sequence. *NMR Biomed.* 2016;29(10):1486-1496.

Table

Table 1: Accuracy and Precision of T_1 values in four tubes with the two T_1 mapping sequences of mIR-rt and MOLLI in phantom study.

No.	Ref (ms)	Accuracy (ms)		Precision	
	IR-SE	mIR-rt	MOLLI	mIR-rt	MOLLI
1	1235	76	166	12.45	8.47
2	1485	120	231	9.31	8.29
3	1885	125	162	20.64	17.32
4	950	66	86	8.87	7.87

Table 2: The T_1 values using mIR-rt sequence from two separate scans for reproducibility analysis.

Subject No.	First Scan (ms)			Second Scan (ms)		
	Apex	Middle	Base	Apex	Middle	Base
1	1574	1557	1529	1584	1570	1541
2	1519	1497	1542	1523	1506	1512
3	1534	1501	1590	1519	1510	1586
4	1577	1554	1518	1549	1558	1551
5	1520	1531	1574	1587	1528	1555
6	1505	1522	1510	1516	1523	1539
Average	1538	1527	1544	1546	1533	1547

Figure captions

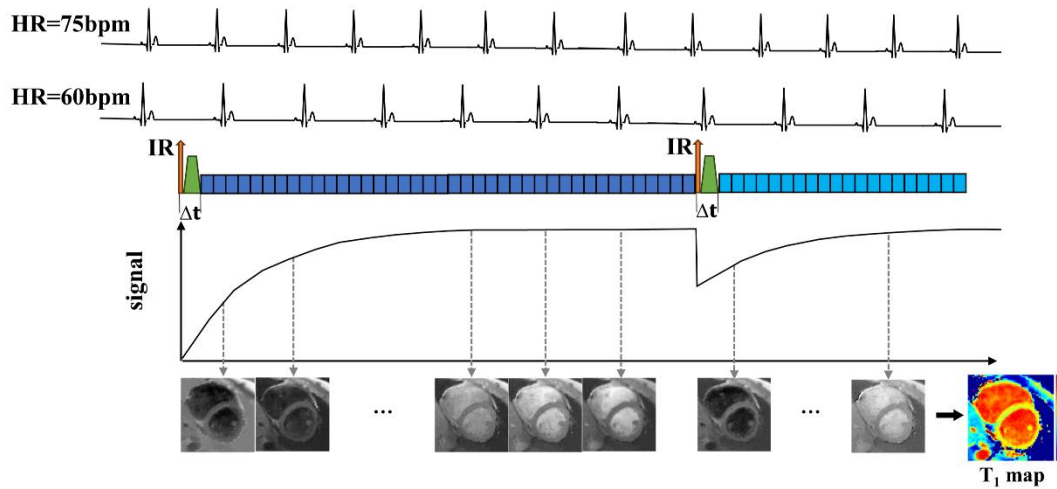


Figure 1. The time diagram of the mIR-rt sequence. The acquisition time of the sequence is fixed at 10.2 seconds. The number of cardiac cycles covered varies with heart rate. Higher heart rates cover more cycles, while lower rates cover fewer. The top two curves are ECG curves of different heart rate cycles. Red arrows are inversion pulses. “ Δt ” (5.8ms) represents the time interval between the IR pulse and the first K-space line. Green trapezoidal blocks represent this interval. Blue bars represent image acquisition. Two inversion pulses are applied in a single breath-hold followed by real-time GRE acquisition. Diastolic images are selected and fitted to obtain T_1 map based on Look-Locker model.

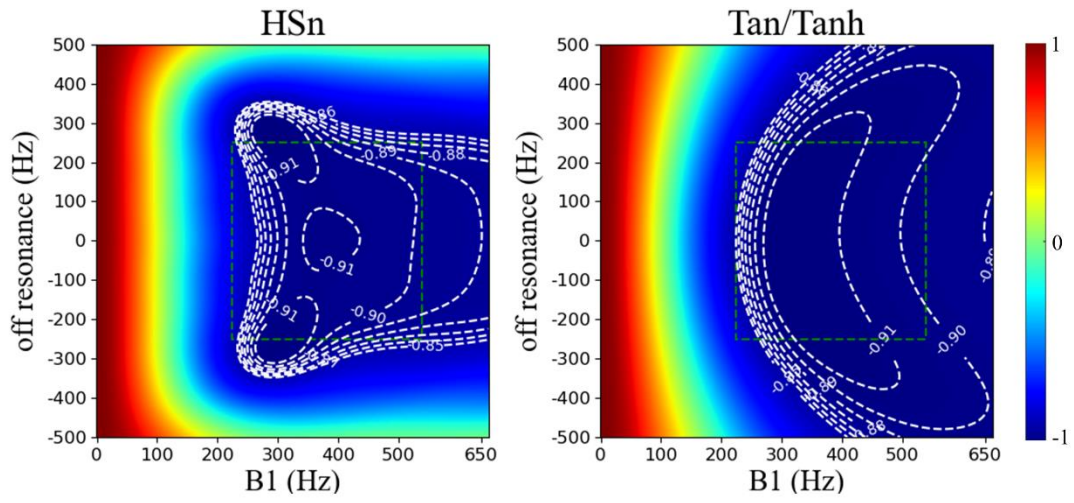


Figure 2. The InvE maps of the best HSn and Tan/Tanh designs over a variety of B_0 and B_1 ranges (B_0 range: -250-250kHz and B_1 range: 225-540kHz). The white dot contours indicate the isometric InvE and the green dot squares denote the desired B_0 and B_1 space.

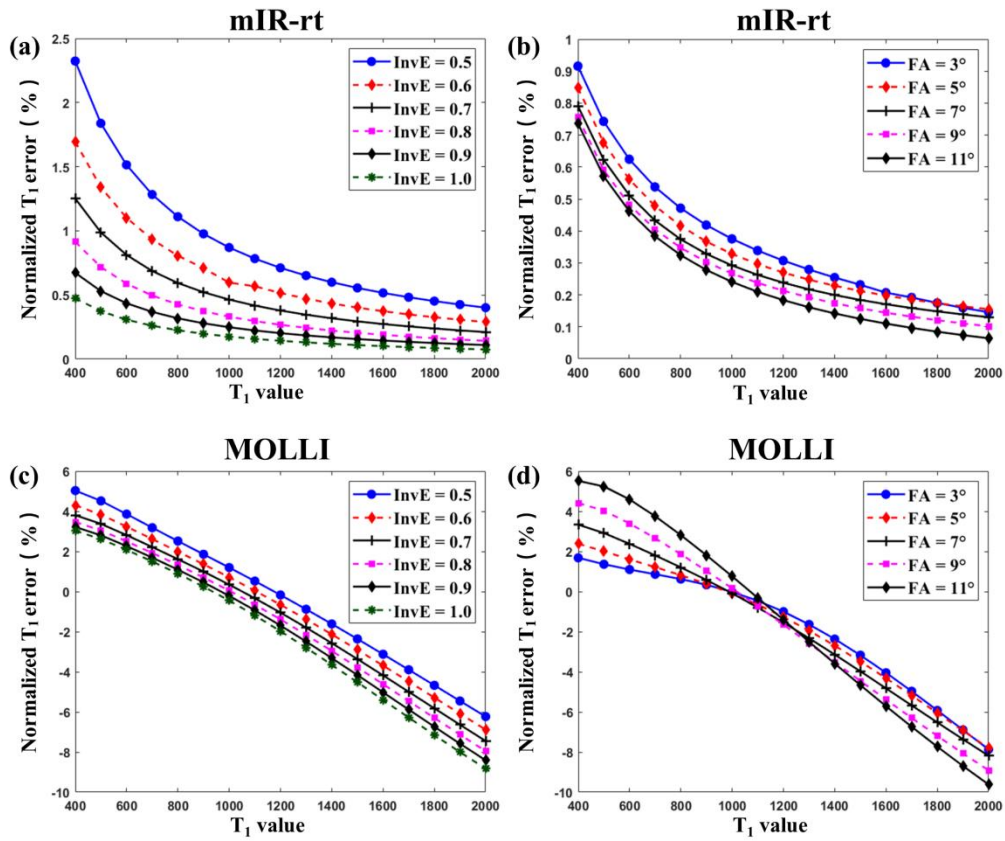


Figure 3. Simulation Results (a) T₁ estimation errors of mIR-rt under different InVEs and T₁ values; (b) T₁ errors of mIR-rt varying with different FAs; (c) T₁ estimation errors of MOLLI under different InVEs and T₁ values; (d) T₁ errors of MOLLI varying with different FAs. The normalized T₁ errors of mIR-rt are less than 1% for T₁ values larger than 1000 ms, while MOLLI underestimates T₁ measurement in the case of long T₁ due to incomplete recovery.

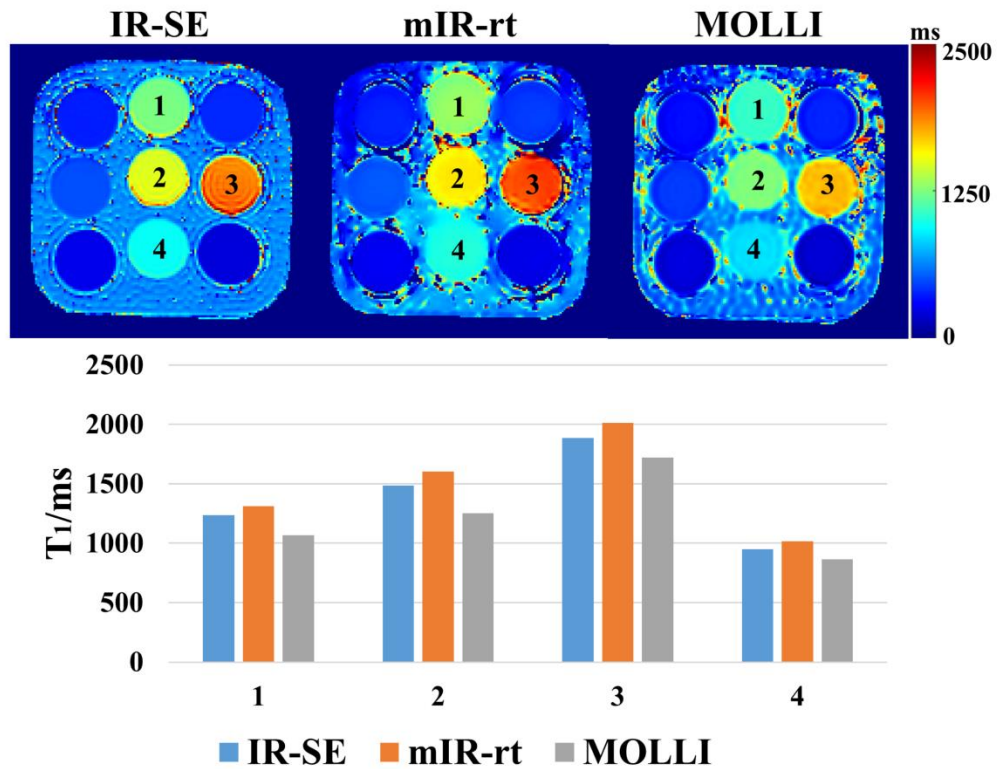


Figure 4. The bar graph of T_1 values obtained from IR-SE, mIR-rt, and MOLLI sequences in the phantom study. The error lines labeled on the mIR-rt and MOLLI histograms represent the standard deviation. The T_1 values of mIR-rt are close to the reference values of IR-SE, while the T_1 values of MOLLI are much lower than the reference values, especially for the fifth and sixth tubes with long T_1 values.

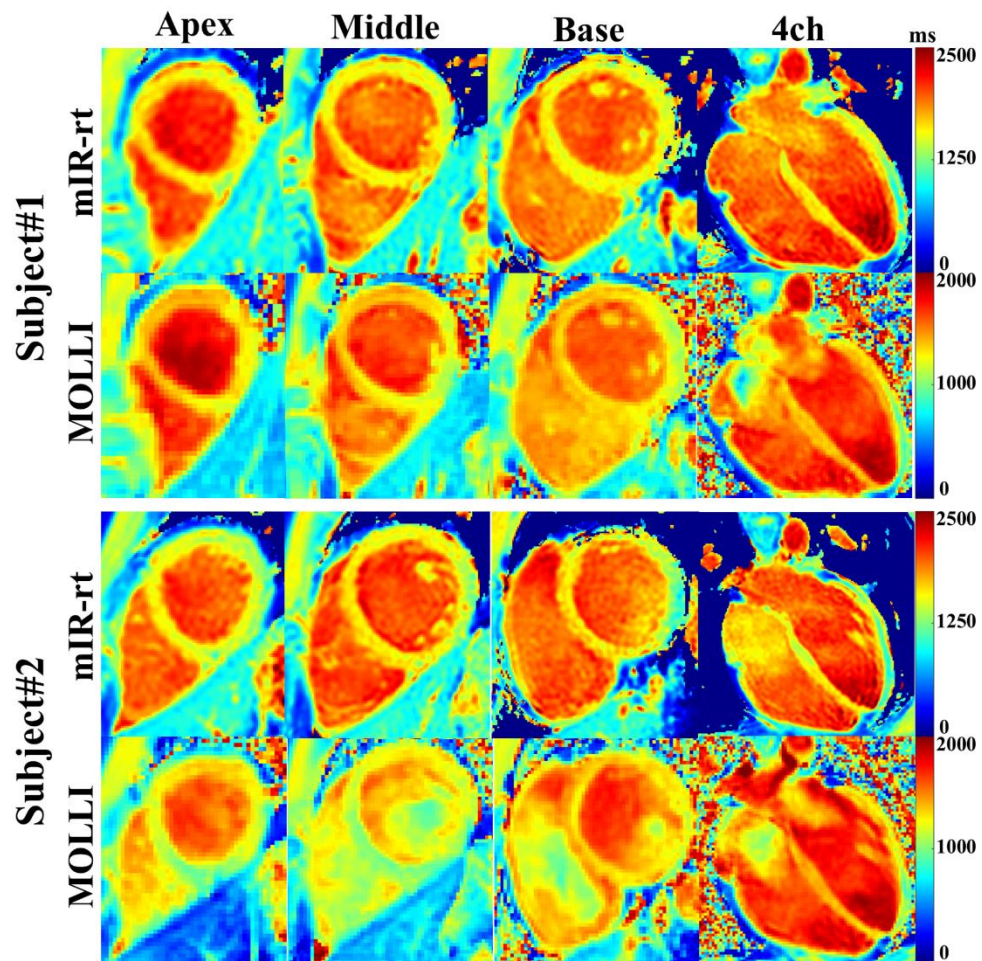


Figure 5. The representative T_1 maps of the short-axis and four-chamber from two volunteers using mIR-rt and MOLLI.

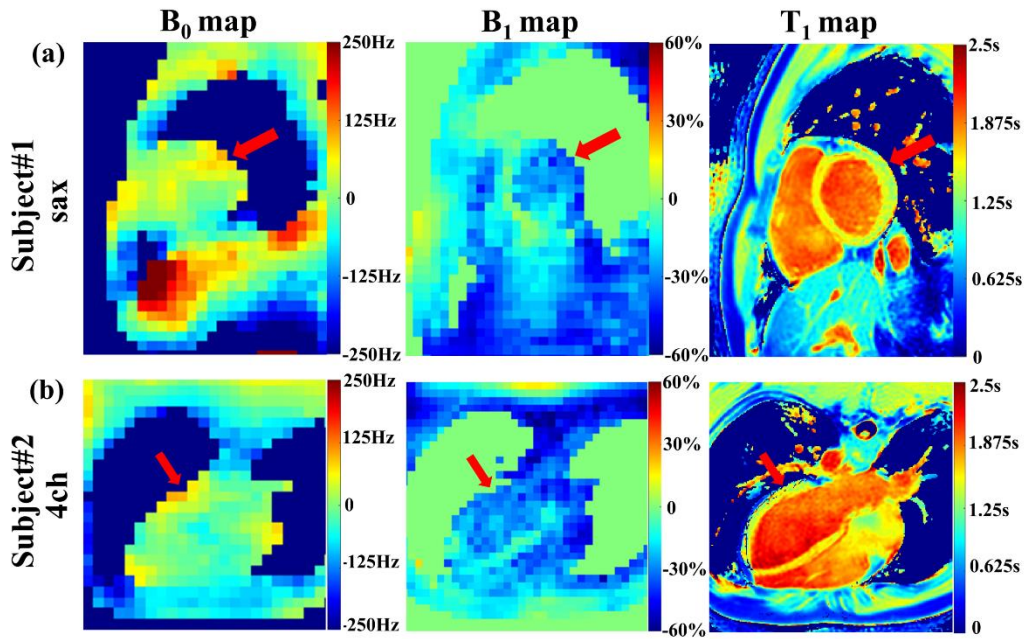


Figure 6. The representative T_1 maps alongside their corresponding B_0 and B_1 maps of the short-axis and four-chamber. The red arrows indicate that a lower B_1 value on the lateral wall results in a lower T_1 value in that area.

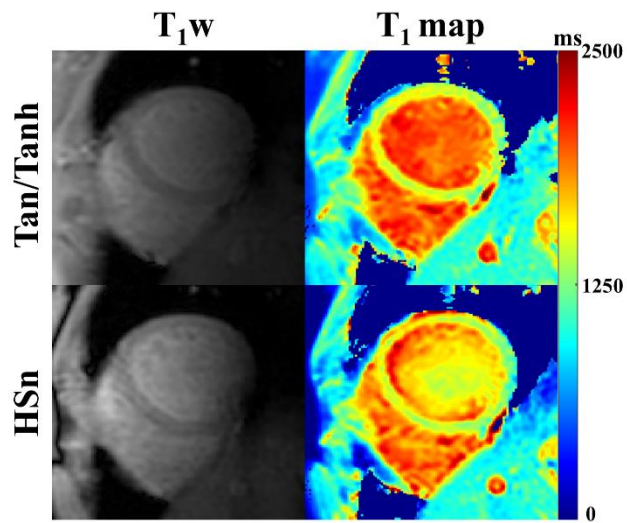


Figure 7. The corresponding T_1 -weighted images and T_1 maps of Tan/Tanh and HSn. From the T_1 map, it can be seen that the blood pool uniformity of Tan/Tanh is better, while the blood flow of HSn has obvious artifacts. Moreover, by comparing T_1 -weighted image and T_1 map image, the T_1 value of HSn has obvious deviation.

Supporting Information captions

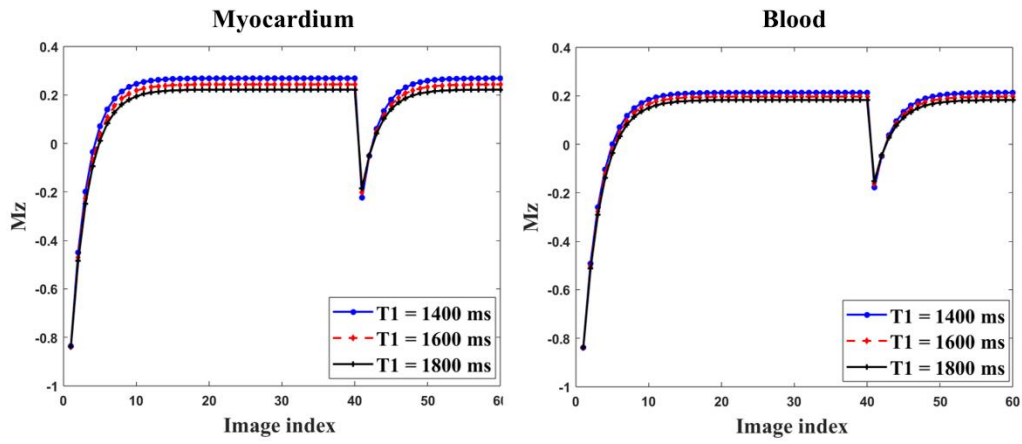


Figure S1. The simulated curves of magnetization of myocardium and blood. The T_1 values were set from 1400ms to 1800ms with an increment of 200ms for the myocardium and were set from 1900ms to 2300ms with an increment of 200ms for the blood pool. From the simulation curve, it is obvious that the spins have reached the steady state before the second IR pulse.

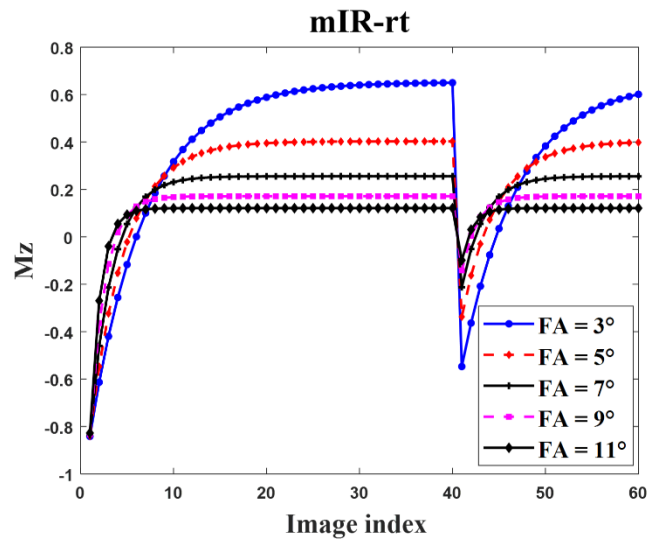


Figure S2. The simulated curves of longitudinal magnetization. Longitudinal magnetization curves at varying FAs from 3° to 11° . Steady-state signal of GRE before the second IR as FA increases. Dynamic range reduction in T_1 -weighted images caused by higher FAs. SNR reduction and its impact on T_1 accuracy. The increased FA reduces the steady-state signal, leading to a decreased dynamic range and lower SNR in the T_1 -weighted images, ultimately affecting the accuracy of T_1 estimation.

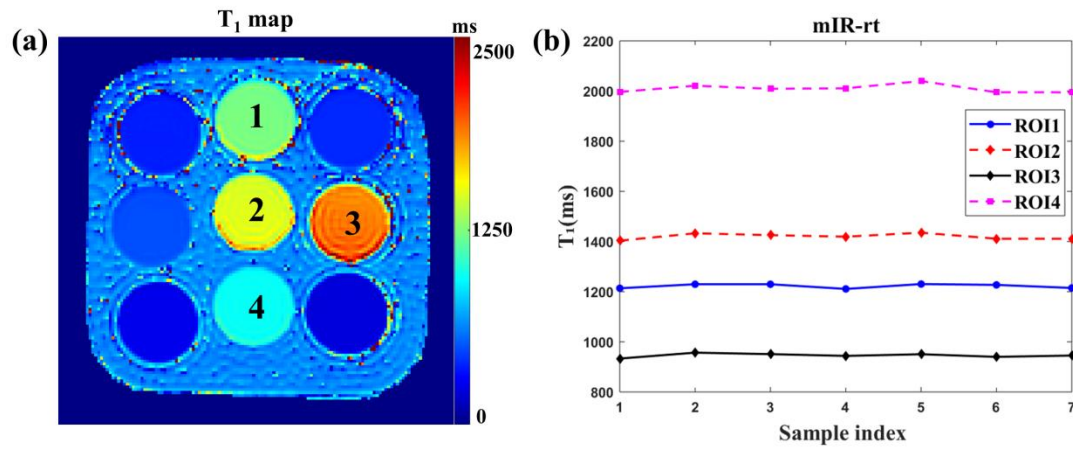


Figure S3. The simulation experiment to investigate the impact of heart rate on T_1 estimates using the mIR-rt sequence. (a) The positions of the four tubes are clearly marked in the T_1 map using the IR-SE sequence. (b) ROI1, ROI2, ROI3, and ROI4 are the regions of interest outlined by the four tubes respectively (corresponds to Figure 4 in the manuscript). The four lines represent the T_1 values of the phantom measured by seven repeated experiments. The results indicate that heart rate has little effect on the estimated T_1 with mIR-rt.